

1 **The role of miniaturisation in the evolution of the mammalian jaw and middle ear**

2

3 Stephan Lautenschlager^{1,2*}, Pamela Gill^{1,3}, Zhe-Xi, Luo⁴, Michael J. Fagan⁵, Emily J.

4 Rayfield^{1*}

5

6 ¹School of Earth Sciences, University of Bristol, UK

7 ²School of Geography, Earth and Environmental Sciences, University of Birmingham, UK

8 ³Earth Science Department, The Natural History Museum, London, UK

9 ⁴Department of Organismal Biology and Anatomy, University of Chicago, USA

10 ⁵School of Engineering and Computer Science, University of Hull, UK

11

12 *Corresponding authors: s.lautenschlager@bham.ac.uk, e.rayfield@bristol.ac.uk

13

14 **The evolution of the mammalian jaw is one of the most important innovations in**
15 **vertebrate history, underpinning the exceptional radiation and diversification of**
16 **mammals over the last 220 million years^{1,2}. In particular the mandible's transformation**
17 **to a single tooth-bearing bone and the emergence of a novel jaw joint while**
18 **incorporating some of the ancestral jaw bones into the mammalian middle ear is often**
19 **cited as a classic textbook example for the repurposing of morphological structures^{3,4}.**
20 **Although remarkably well documented in the fossil record, the evolution of the**
21 **mammalian jaw still poses an intriguing paradox: how could bones of the ancestral jaw**
22 **joint function both as a joint hinge for powerful load bearing mastication and also as**
23 **mandibular middle ear that would be delicate enough for hearing? Here, we use new**
24 **digital reconstructions, computational modelling, and biomechanical analyses to**
25 **demonstrate that miniaturisation of the early mammalian jaw was the primary driver**

26 **for the transformation of the jaw joint. We show that there is no evidence for a**
27 **concurrent reduction in jaw joint stress and a simultaneous increase in bite force in key**
28 **non-mammaliaform taxa in the cynodont-mammaliaform transition as previously**
29 **thought⁵⁻⁸. Although a shift in the recruitment of the jaw musculature occurred during**
30 **the evolution to modern mammals, the optimisation of the mandibular function to**
31 **increase bite force while reducing joint loads did not occur until after the emergence of**
32 **the neomorphic mammalian jaw joint. This suggests that miniaturisation provided a**
33 **selective regime for the evolution of the mammalian jaw joint, followed by the**
34 **integration of the postdentary bones into the mammalian middle ear.**

35 The mammalian jaw and jaw joint are unique among vertebrates⁶. While the
36 craniomandibular jaw joint (CMJ) of non-mammalian vertebrates is formed between the
37 quadrate and articular bones, mammals evolved a novel jaw hinge between the squamosal
38 and dentary bones (secondary/temporomandibular jaw joint, TMJ)¹⁻⁴. The evolutionary
39 origins of this morphological transformation involved a suite of osteological modifications to
40 the feeding and auditory systems, occurring over a period of 100 million years during the
41 Late Triassic and Jurassic across the cynodont-mammaliaform transition^{9,10}. The tooth-
42 bearing dentary bone increased in size relative to the postdentary elements, eventually
43 transforming the seven-bone lower jaw in pre-mammalian cynodonts (referred to as
44 cynodonts hereafter) to a single-bone jaw in modern mammals; parallel to this simplification
45 of the mandible, the integration of elements of the ancestral CMJ into the ossicular chain led
46 to a unique middle and inner ear morphology capable of more sensitive sound detection^{11,12}.
47 While new fossil information has suggested that a definitive mammalian middle ear (DMME)
48 evolved independently in at least three mammalian lineages by detachment from the
49 mandible, the emergence of a secondary jaw joint is a key innovation uniting all
50 mammaliaforms^{9,13}. However, a central question exists as to how the jaw hinge remained to

51 be robust enough to bear strong mastication forces, while the same bones in the jaw would
52 become delicate enough to be biomechanically viable for hearing, during this
53 transformation^{3,5,10}.

54 The stepwise acquisition of morphological features leading to the emergence of the
55 TMJ is exceptionally well documented in the fossil record by a series of transitional taxa
56 illuminating the evolutionary dynamics involved⁴. Whilst still appearing to function as a jaw
57 joint and viable for sound transmission in cynodonts (e.g. *Thrinaxodon liorhinus*,
58 *Probainognathus*, *Probelesodon sanjuanensis*), the postdentary bones gradually reduced in
59 size and shifted away from the jaw joint – likely for more sensitive hearing^{10,12}. This trend
60 resulted in all basal mammaliaforms (e.g. *Sinoconodon rigneyi*, *Morganucodon oehleri*)
61 possessing a remarkable ‘dual jaw joint’ with two seemingly functional joints: a quadrate-
62 articular joint medial to a mammalian dentary condyle and squamosal glenoid hinge^{11,13}.
63 More derived groups and crown mammals eventually lost the ancestral quadrate-articular
64 joint. In addition to fossil evidence, this sequence of events was identified historically in
65 embryonic stages of living mammals^{14,15} and recent morphogenetic studies, gene patterning
66 and regulatory networks have elucidated the development of these structures further^{16,17}.
67 Previous studies have theorised that muscle reorganisation reduced load at the jaw joint^{6,10},
68 yet these claims have not been tested in fossil taxa and experimental studies of extant
69 mammals reveal that the jaw joint usually experiences net compressive loading^{18,19}. The
70 modification of the mandible and the emergence of a novel jaw joint and middle ear,
71 therefore, represents an intriguing problem. This is especially puzzling when all the evidence
72 points towards modifications for increased jaw muscle force, consolidation of cranial bones,
73 increased complexity of sutures and supposedly stronger skulls during mammalian
74 evolution^{1,5}.

75 Here, we have integrated a suite of digital reconstruction, visualisation and
76 quantitative biomechanical modelling techniques to test the hypothesis that reorganisation of
77 the adductor musculature and reduced stress susceptibility in the ancestral jaw joint
78 facilitated the emergence of the mammalian TMJ. Applying finite element analysis (FEA),
79 we calculated bone stress, strain and deformation to determine the biomechanical behaviour
80 of the mandibles of six key taxa across the cynodont-mammaliaform transition (Fig 1). These
81 analyses were supplemented by multibody dynamics analysis (MDA) to predict bite forces
82 and joint reaction forces. Results from the combined analyses demonstrate that during
83 simulated biting there is no evidence for the reduction of stresses (von Mises, tensile,
84 compressive) in the jaw joint (CMJ and/or TMJ) across the studied cynodont and
85 mammaliaform taxa (Figs. 2, 3, Extended data figs. 1, 3). This was found for unilateral and
86 bilateral biting simulations and regardless of the working and balancing side joint. However,
87 bite position appears to have a moderate effect on joint stresses (particularly compression),
88 with stress increasing as the bite point moves anteriorly along the tooth row. This is
89 consistent with experimental data for extant mammals, in which incisor biting resulted in the
90 highest joint loads²⁰. Similarly, MDA results show that absolute joint reaction forces are not
91 reduced while the jaw joint underwent morphological transformation (Figs. 2, 3), whereas
92 relative bite forces (ratio between muscle force and bite force) are found to decrease in
93 derived cynodonts (*Probainognathus* and crownwards) and to stay largely constant in
94 mammaliaforms, such as *Morganucodon oehleri* and *Hadrocodium wui* (Extended data figs
95 1-3). However, the simulation of different muscle activation patterns using FEA reveals that
96 there is, across the cynodont-mammaliaform transition, a distinct shift in the recruitment of
97 jaw adductor musculature required to achieve high bite forces that maintain low stress in the
98 jaw joint (Fig. 4a). The highest bite forces while keeping joint tensile stresses low are found
99 for jaw adduction dominated by the masseter muscle group in the cynodonts *Thrinaxodon*

100 *liorhinus*, *Diademodon tetragonus* and *Probainognathus* sp. In *Probelesodon sanjuanensis*
101 and the mammaliaforms *Morganucodon oehleri* and *Hadrocodium wui* the recruitment of the
102 pterygoideus muscle group (with contribution of the masseter musculature) provides the
103 highest relative bite forces, eventually shifting to the temporalis group as the dominant
104 contributor for high bite force/low joint stress performance in the extant taxon *Monodelphis*
105 *domestica*. This pattern is reversed for muscle activations optimised for high bite force in
106 relation to low compressive stresses in the jaw joint in mammaliaforms in comparison to
107 cynodonts (Fig. 4a). While this is achieved mainly by recruitment of the temporalis group in
108 cynodonts, the masseter and the pterygoideus groups form the dominant musculature in
109 mammaliaforms. Apart from an overall shift in the pattern of muscle recruitment, the
110 analyses further demonstrate that while in the cynodonts and mammaliaforms a single muscle
111 group is harnessed to achieve ‘optimal’ bite forces (i.e. high bite force/low jaw joint stress),
112 *Monodelphis domestica* simultaneously activates all three muscles groups (Extended data
113 figs. 4-9) as revealed by the computational analyses here, confirming previous experimental
114 data²¹. Changes to muscle orientation and inferred muscle lines of action either precede or are
115 associated with mandible shape change²², leading to a more efficient use of the adductor
116 system to maximise bite force and minimise loads on the jaw joint.

117 Considering that the shape of the mandible alone does not appear to have a substantial
118 influence on stress reduction in the mandibles of the studied taxa, we further tested size-
119 related effects on the biomechanical behaviour of the jaw joint. All taxa were scaled to seven
120 different jaw lengths (5-320 mm) covering the mandibular size range observed across the
121 cynodont-mammaliaform transition (Fig. 1, Fig. 4b, supplementary table S1). Results for
122 these hypothetical resized models demonstrate that absolute tensile and compressive stresses
123 in the jaw joint decrease exponentially to 25% with a reduction in size by 50%. At the same
124 time, absolute bite forces decrease by 50%, in direct proportion to jaw length.

125 We offer new biomechanical evidence that stress susceptibility of the mandible, and
126 in particular of the jaw joint, was not reduced across the cynodont-mammaliaform transition.
127 This contrasts with existing hypotheses that argue for a reduction of joint loads due to the
128 rearrangement of the jaw adductor musculature and the resultant increase in bite force in
129 mammaliaforms^{1,7,8}. The decrease in size of the postdentary bones and the accompanying
130 expansion of bony angular and coronoid projections of the dentary is assumed to have
131 paralleled the reorganisation and evolution of mammalian muscle groups (masseter and
132 temporalis)^{6,8,21}. Arranged in such a manner, the changed line of action of the major jaw
133 adductor muscles was hypothesised to have led to a redistribution of muscle forces with little
134 or no load experienced at the jaw hinge. However, our results do not support these previous
135 inferences.

136 As demonstrated here, a change in the recruitment of the jaw adductor musculature
137 can be observed to achieve high bite forces, while at the same time keeping tensile and
138 compressive joint stresses at a minimum. These findings parallel experimental data from
139 extant mammals that differential muscle activation produces different stress regimes in the
140 jaw joint²⁰. However, in the studied cynodonts and mammaliaforms, parallel activation of all
141 three adductor muscle groups does not lead to the highest relative bite forces (Extended data
142 figs. 4-9) as found in *Monodelphis domestica*. Although the mammal-like muscle division
143 and arrangement of the jaw adductors preceded the osteological transformation of the
144 mandible and jaw joint²¹, it was not until a later stage in mammalian evolution that further
145 optimisations to muscle function occurred. A recent study²³ using free-body analysis of the
146 cynodont lower jaw confirmed that the musculoskeletal system was morphologically and
147 evolutionary flexible without negatively impacting functional performance.

148 Rather than alterations of the osteology and the muscular arrangement, reduction in
149 mandibular size produced the most notable effects on minimising absolute jaw joint stress in

150 our analyses. Although a decrease in size leads to two conflicting trends of reducing tensile
151 and compressive stresses but also bite forces, stress reduction is achieved at a higher rate than
152 bite force reduction (exponential vs linear). Consequently, our biomechanical analyses
153 predict that smaller mandibular size constitutes the best compromise to ameliorate loss of bite
154 force and stress reduction in the jaw joint. This prediction is corroborated by the reduction in
155 size in the vast majority of taxa phylogenetically intermediate in the cynodont-
156 mammaliaform transition, in which such a biomechanical compromise was achieved (Fig. 1,
157 4b). Miniaturisation has been discussed as a key factor during the evolution of mammals in
158 the context of thermoregulation, nocturnality and dietary/ecological adaptations^{1,2,24,25}. It has
159 further been proposed to be a structural requirement for the acquisition of mammalian
160 characters¹. While size-related stress reduction might not have been the main target for
161 selection, it could have constituted a by-product of adaptation to a specific ecological niche
162 demanding small body size²⁶ during early phases of radiation^{4,27}. Our results demonstrate that
163 changes to joint morphology and muscle (re-)organisation have little impact on joint loading.
164 Instead, reduction in size appears to be key, by lowering stress and strain disproportionately
165 to bite force magnitude. Miniaturisation of the mandibular system could, therefore, be a
166 crossing of an evolutionary Rubicon, in the emergency of the TMJ, and in further functional
167 integration of postdentary bones in the middle ear, before their final separations from the
168 mandible in respective lineages, leading to a spectacular diversification of crown mammals.
169

- 170 1. Kemp, T. S. *The Origin and Evolution of Mammals* (Oxford Univ. Press, Oxford, 2005).
171 2. Kielan-Jaworowska, Z. et al. *Mammals from the Age of Dinosaurs—Origins, Evolution,
172 and Structure* (Columbia Univ. Press, New York, 2004).

- 173 3. Crompton, A. W. Evolution of the jaw articulation in cynodonts *in* Joysey, K. A. &
174 Kemp, T. S. *Studies in Vertebrate Evolution*. (Oliver & Boyd, Edinburgh, 1972), 231-
175 253.
- 176 4. Luo, Z.-X. Transformation and diversification in early mammal evolution. *Nature*. **450**,
177 1011–1019 (2007).
- 178 5. Crompton, A.W., Hylander, W. L. Changes in mandibular function following the
179 acquisition of a dentary-squamosal joint. *in The Ecology and Biology of Mammal-like*
180 *Reptiles* (eds N. Hotton III, P. D. MacLean, J. J. Roth, E. C. Roth, Smithsonian
181 Institution Press, Washington.), 263-282 (1986).
- 182 6. Bramble, D. M. Origin of the mammalian feeding complex: models and mechanisms.
183 *Paleobiology* **4**, 271-301 (1978).
- 184 7. Barghusen, H. R. *in Morphology of the maxillomandibular apparatus* (ed G. H.
185 Schumacher) 26-32 (VEB Georg Thieme, 1972).
- 186 8. DeMar, R. & Barghusen, H. R. Mechanics and the evolution of the synapsid jaw.
187 *Evolution* **26**, 622-637 (1972).
- 188 9. Luo, Z.-X. Developmental patterns in Mesozoic evolution of mammal ears. *Ann. Rev.*
189 *Ecol. Evol. Syst.* **42**, 355-380 (2011).
- 190 10. Allin, E. F. Evolution of the mammalian middle ear. *J. Morph.* **147**, 403-437 (1975).
- 191 11. Sidor, C. A. Evolutionary trends and the origin of the mammalian lower jaw.
192 *Paleobiology* **29**, 605-640 (2003).
- 193 12. Manley, G. A. Evolutionary paths to mammalian cochleae. *J. Assoc. Res.*
194 *Otolaryngology* **13**, 733-743 (2012).
- 195 13. Luo, Z.-X., et al. New evidence for mammaliaform ear evolution and feeding adaptation
196 in a Jurassic ecosystem. *Nature* **548**, 326 (2017).

- 197 14. Reichert, C. Über die Visceralbogen der Wirbelthiere im Allgemeinen und deren
198 Metamorphosen bei den Vögeln und Säugethieren. *Archiv für Anatomie, Physiologie und*
199 *wissenschaftliche Medicin*, 120-222 (1837).
- 200 15. Gaupp, E. W. T. Die Reichertsche Theorie (Hammer-, Amboss und Kieferfrage). *Archiv*
201 *für Anatomie und Entwicklungsgeschichte* **1912**, 1–426 (1913).
- 202 16. Urban, D. J. et al. A new developmental mechanism for the separation of the mammalian
203 middle ear ossicles from the jaw. *Proc. R. Soc. B* **284**, 20162416 (2017).
- 204 17. Anthwal, N. et al. Meckel's cartilage breakdown offers clues to mammalian middle ear
205 evolution. *Nature Ecol. Evol.* **1**, (2017).
- 206 18. Hylander, W. L. The functional significance of primate mandibular form. *J. Morph.* **160**,
207 223-239 (1979)
- 208 19. Herring, S. W., Rafferty, K. L., Liu, Z. J., & Marshall, C. D. Jaw muscles and the skull in
209 mammals: the biomechanics of mastication. *Comp. Biochem. Phys. A.* **131**, 207-219
210 (2001).
- 211 20. Liu, Z.J. & Herring, S.W. Bone surface strains and internal bony pressures at the jaw
212 joint of the miniature pig during masticatory muscle contraction. *Arch. Oral Bio.* **45**, 95-
213 112 (2000).
- 214 21. Crompton, A. W. in *Functional Morphology in Vertebrate Paleontology* (ed J. J.
215 Thomason) 55-75 (Cambridge University Press, 1995).
- 216 22. Lautenschlager, S. et al. Morphological evolution of the mammalian jaw adductor
217 complex. *Biol. Rev.* **92**, 1910-1940 (2017).
- 218 23. Reed, D. A. Iriarte-Diaz, J., Diekwisch, T. G. H. A three dimensional free body analysis
219 describing variation in the musculoskeletal configuration of the cynodont lower jaw.
220 *Evol. Develop.* **18**, 41-53 (2016).

- 221 24. Rowe, T. Phylogenetic systematics and the early history of mammals. In *Mammal*
222 *Phylogeny* (pp. 129-145). Springer New York, (1993).
- 223 25. Kemp, T. S. The origin of higher taxa: macroevolutionary processes, and the case of the
224 mammals. *Acta Zool.* **88**, 3-22 (2007).
- 225 26. Hanken, J., & Wake, D. B. Miniaturization of body size: organismal consequences and
226 evolutionary significance. *Ann. Rev. Ecol. Syst.* **24**, 501-519 (1993).
- 227 27. Gill, P. *et al.* Dietary specializations and diversity in feeding ecology of the earliest stem
228 mammals. *Nature* **512**, 303-307 (2014).
- 229 28. Close, R. A., Friedman, M., Lloyd, G. T., & Benson, R. B. Evidence for a mid-Jurassic
230 adaptive radiation in mammals. *Current Biology* **25**, 2137-2142, (2015).
- 231 29. Pacheco, C. P., Martinelli, A. G., Pavanatto, A. E., Soares, M. B., & Dias-da-Silva, S.
232 *Prozostrodon brasiliensis*, a probainognathian cynodont from the Late Triassic of Brazil:
233 second record and improvements on its dental anatomy. *Historical Biology* 1-11, (2017).

234

235 **Acknowledgments** We thank P. Brewer, S. Chapman (Natural History Museum, London), O.
236 Rauhut, G. Roessner (Bayerische Staatssammlung fuer Historische Geologie und
237 Palaeontologie, Munich), K. Angielczyk, W. Simpson (Field Museum of Natural History,
238 Chicago), G. Hantke and A. Kitchener (National Museums of Scotland, Edinburgh) for
239 access to specimens in their care. T. Rowe and J. Maisano (University of Texas, Austin)
240 generously provided digital data sets of specimens. A. Neander (University of Chicago), G.
241 Roessner (Bayerische Staatssammlung fuer Historische Geologie und Palaeontologie,
242 Munich), D. Sykes (Natural History Museum London), K. Robson Brown (University of
243 Bristol), O.Katsamenis and M. Mavrogordato (University of Southampton) assisted with CT
244 scanning. J. Hopson (University of Chicago) is thanked for discussion. Three anonymous
245 reviewers are thanked for helpful suggestions improving earlier manuscript versions. This

246 work was funded by NERC (Natural Environment Research Council) grants NE/K01496X/1
247 (to E.J.R.) and NE/K013831/1 (to M.J.F.), and support from the University of Chicago (to Z.-
248 X. L).

249

250 **Contributions**

251 S.L., P.G., Z.-X. L., M.F and E.R. conceived and designed the study. S.L., P.G., Z.-X. L., and
252 E.R. arranged logistics of specimens for CT scanning and collected CT data. Z.-X. L.
253 provided access to additional specimens and data. S.L. processed CT data, performed digital
254 restorations and reconstructions, performed computational analyses. M.F and E.R.
255 contributed to FEA and MDA analyses. S.L., P.G., Z.-X. L., M.F and E.R equally contributed
256 to the analysis of results. S.L. prepared main text, figures and supplementary data. S.L., P.G.,
257 Z.-X. L., M.F and E.R equally contributed to editing, commenting and revising the
258 manuscript and figures. M.F. and E.R. acquired funding.

259 **Competing interests**

260 The authors declare no competing interests.

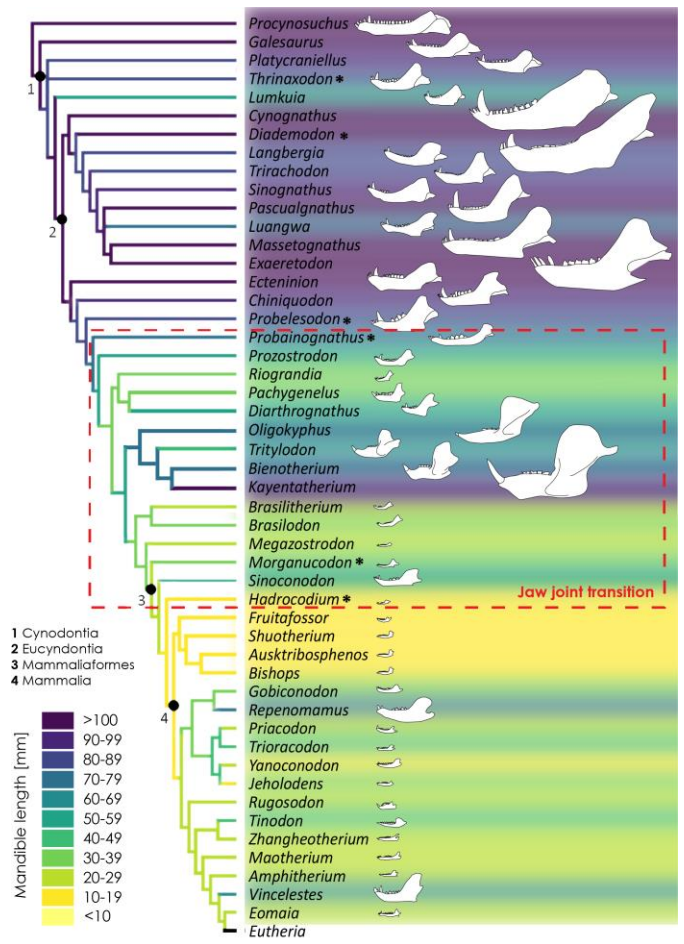
261 **Corresponding author**

262 Correspondence to Stephan Lautenschlager (s.lautenschlager@bham.ac.uk) or Emily
263 Rayfield (e.rayfield@bristol.ac.uk)

264

265 **Data availability.** All relevant data (three-dimensional osteological, FEA and MDA models)
266 are made available via the University of Bristol's DataBris repository.

267

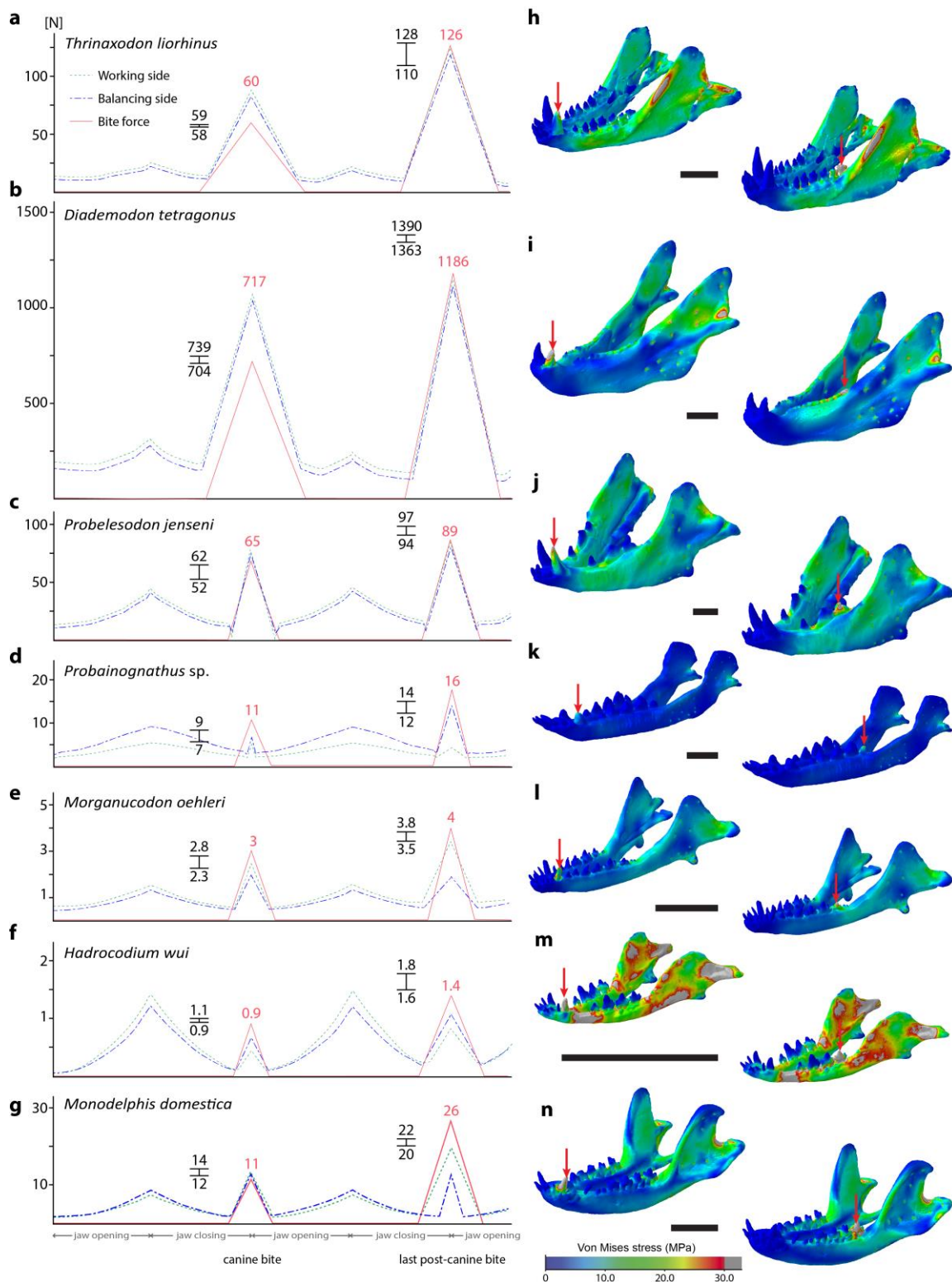


269

270 **Figure 1 | Mandibular sizes and evolutionary relationships of cynodonts,**
 271 **mammaliaforms and mammals.** Asterisk denotes studied taxa. Phylogeny simplified after
 272 Luo et al.¹³, Close et al.²⁸ and Pacheco et al.²⁹.

273

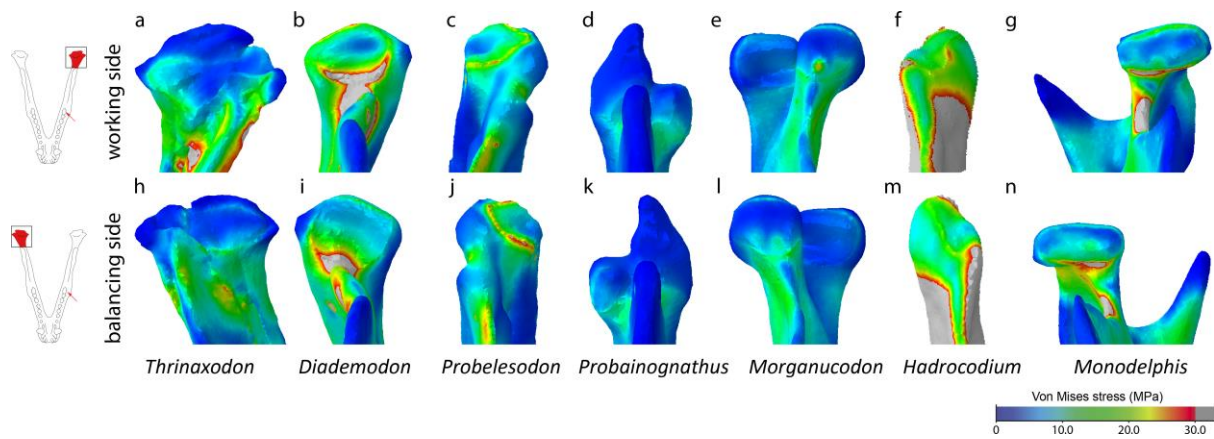
274



275

276 **Figure 2 | Biomechanical analysis of cynodont and mammaliaform taxa for simulated**
 277 **unilateral biting at canines and most posterior tooth. a-g, MDA plots showing bite forces**
 278 **and joint forces (working and balancing side) during jaw opening and closing cycles. Range**
 279 **bars denote bite force values obtained from the FE models. Peak values in red represent**

280 maximum bite force obtained from MDA models. **h-n**, FE von Mises stress contour plots for
281 bite at canine and last tooth (indicated by red arrows). Scale bars for (h, j-n) 10 mm, (i) 50
282 mm.
283
284

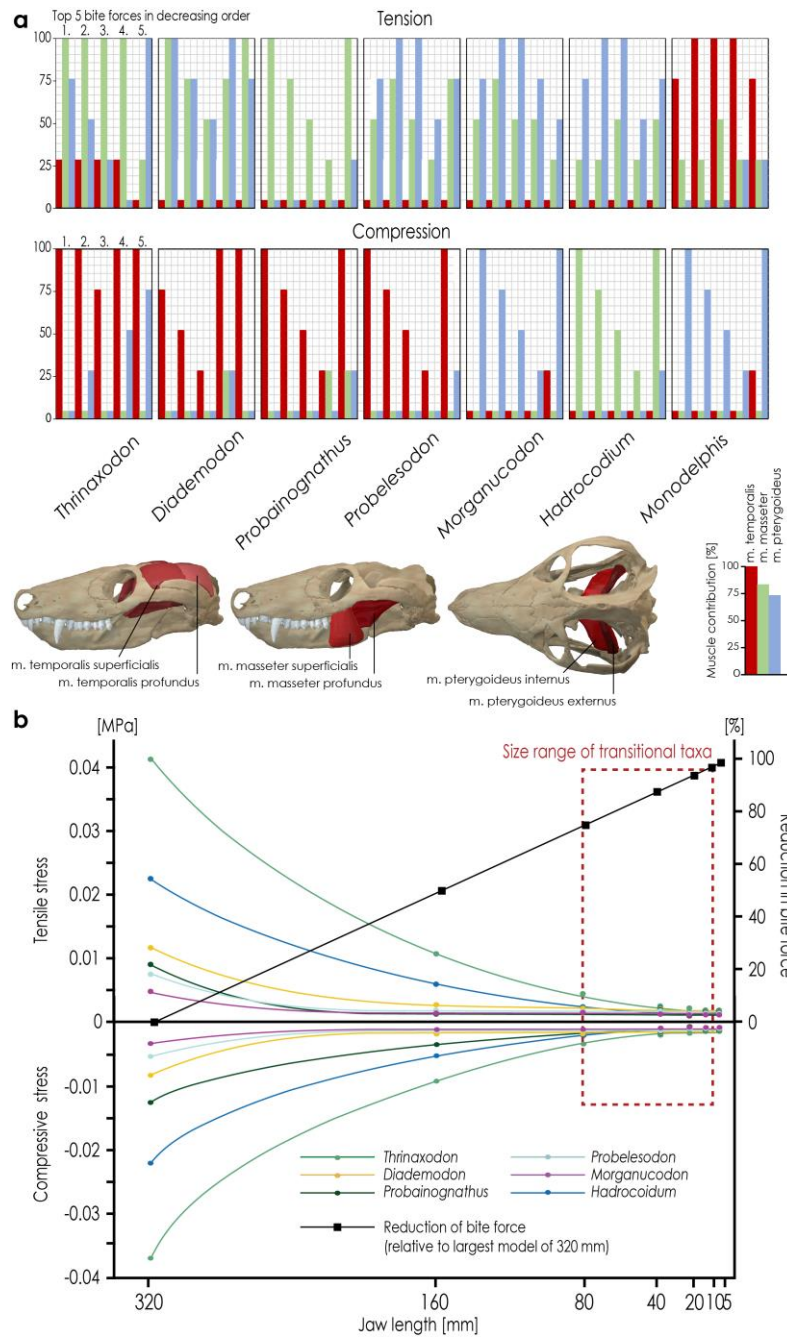


285

286 **Figure 3 | Von Mises stress contour plots of mandibular joint region. a-g,** Jaw joint of the
 287 working side in dorsal view, **h-n,** jaw joint of the balancing side in dorsal view. All contour
 288 plot images scaled to the same size. Results shown for simulated unilateral bite at the most
 289 posterior tooth.

290

291



292

293 **Figure 4 | Muscle activation patterns and joint stress calculations a,** Muscle activation
 294 simulation to achieve highest bite forces relative to minimum tensile and compressive stress
 295 at the jaw joint. Muscle combinations for the five highest bite force vs stress outputs shown
 296 for all taxa in decreasing order (1-5). Reconstructed adductor muscle groups depicted in skull
 297 images. **b,** Tensile and compressive stresses in the jaw joint and percentage reduction ('loss')
 298 in bite force (relative to largest model of 320mm) of all taxa, each scaled to seven different

299 jaw lengths. Relative bite force reduction is the same for all models with each successive size
300 and represented by a single trend line.

301

302 **METHODS**

303 **Specimens and digital models.** Three-dimensional digital models of key cynodont and
304 mammaliaform taxa were created for this study using the following specimens: *Thrinaxodon*
305 *liorhinus* (NHMUK PV R 511, 511a, Natural History Museum, London, UK), *Diademodon*
306 *tetragonus* (BSP 1934 VIII 17/2, Bayerische Staatssammlung für Historische Geologie und
307 Paläontologie, Munich, Germany), *Probelesodon sanjuanensis* (PVSJ 411, Museo de
308 Ciencias Naturales, Universidad Nacional de San Juan, Argentina), *Probainognathus* sp.
309 (PVSJ 410), *Morganucodon oehleri* (FMNH CUP 2320, Field Museum of Natural History,
310 Chicago, USA; IVPP 8685, Institute for Vertebrate Palaeontology and Palaeoanthropology),
311 *Morganucodon watsoni* (NHMUK PV M 26144, articulated squamosal and petrosal;
312 NHMUK PV M 92838 & M 92843, isolated quadrates; NHMUK PV M 27410, isolated
313 fragmentary jugal), *Hadrocodium wui* (IVPP 8275), *Monodelphis domestica* (National
314 Museum of Scotland, Edinburgh). All specimens were digitised using CT scanning or (as in
315 the case of *Diademodon tetragonus*) a photogrammetry approach. For scan details see²¹. For
316 the model creation and the removal of taphonomic artefacts, scan data were imported into
317 Avizo (version 8, VSG, Visualisation Science Group). Data sets were segmented manually in
318 Avizo segmentation editor to separate bone from the surrounding matrix. As all fossil
319 specimens exhibited various preservational and taphonomic artefacts, different restoration
320 steps were applied as outlined in detail in Lautenschlager^{22,29}: For a detailed account of the
321 restorative steps of the individual specimens the reader is referred to the supplementary
322 information and Lautenschlager et al.²².

323 Three-dimensional models of the jaw adductor muscle anatomy of all fossil
324 specimens were reconstructed digitally following a protocol outlined in Lautenschlager³⁰.
325 Reconstructions were performed on the basis of osteological correlates indicating muscle
326 attachment sites. Where exact locations and boundaries between adjacent attachments were

327 unclear, topological criteria were applied. Corresponding insertions and origins of each
328 muscle were connected by simple point-to-point connections to evaluate the muscle
329 arrangement and to identify possible intersections or other conflicts. Following this initial
330 reconstruction, muscle dimensions and volumes were modelled according to spatial
331 constraints within the bony structure. Data obtained from contrast-enhanced CT scanning of
332 *Monodelphis domestica* was consulted to further inform the fossil muscle reconstructions.
333 Competing hypotheses regarding the exact placement and arrangement of specific muscles
334 were evaluated by analysing muscle strain^{22,31}. Full details and discussion of the
335 reconstructed jaw adductor complex across the studied taxa can be found in Lautenschlager et
336 al.²². The final muscle reconstructions were used to supply input parameters for the
337 subsequent finite element analysis (FEA) and multibody dynamics analysis (MDA). Muscle
338 forces were calculated based on physiological cross-section area³², which was estimated by
339 dividing the volume of each muscle by its total length (supplementary table S2).

340

341 **Multibody dynamics analysis.** For MDA, the digitally restored models of all taxa were
342 imported into Adams (version 2013.2, MSC Software Corp.) as rigid bodies in .x_t parasolid
343 format. The skull and jaw models were aligned manually to articulate at the quadrate-
344 articular joint or the squamosal-dentary joint, respectively. Throughout all simulations, the
345 skull models were kept immobile; the jaw models were allowed mobility in all degrees of
346 freedom. Skull and jaw models were connected by spherical joint elements in Adams. Mass
347 and inertial properties were calculated in Adams based on rigid body geometry and an
348 average bone density of 1764 kg/m³³³. The different adductor muscle groups were modelled
349 as a series of spring elements linking corresponding muscle insertion and origin sites. Muscle
350 forces were assigned according to the calculations taken from the three-dimensional
351 reconstructions. Muscle activation was modelled by applying a dynamic geometric

352 optimisation (DGO) method³⁴. Unilateral and bilateral biting at the canines and the
353 posteriormost tooth position were simulated using a rigid body box element from the Adams
354 solids library. The box was placed perpendicular to the teeth at the aforementioned tooth
355 positions and moved posteriorly during jaw opening phases. Bite forces and joint reaction
356 forces for the working and balancing side joints (for the unilateral bite scenarios) were
357 recorded throughout the bite simulations.

358 Two sets of simulations were performed for each taxon: (i) all models scaled to the
359 actual size of the physical specimens, (ii) all taxa scaled to the same surface area to evaluate
360 the biomechanical effects of morphological differences independent of size³⁵. For the latter
361 scenario, the model of *Thrinaxodon liorhinus* was selected as the reference as it represents
362 approximately the average size of all models (which range in jaw length between 13mm and
363 270mm); all other models were scaled to the same surface area as the *Thrinaxodon* model.

364

365 **Finite element analysis.** For FEA, jaw models of all taxa were imported into Hypermesh
366 (version 11, Altair Engineering) for the creation of solid mesh FE models and the setting of
367 boundary conditions. All jaw models consisted of approximately 2,500,000 tetrahedral
368 elements. Material properties for mandibular bone and teeth were assigned based on nano-
369 indentation results for hedgehog mandibles (bone: $E = 12 \text{ GPa}$, $\nu = 0.30$, tooth: $E = 25.0 \text{ GPa}$,
370 $\nu = 0.3$); material properties for mammalian mandibular sutures were taken ($E = 46.0 \text{ MPa}$, ν
371 $= 0.35$) from literature data³⁶. Due to the resolution of some CT datasets, cortical and
372 cancellous bone were not differentiated, permitting the use of models derived from different
373 digitisation methods (volumetric: computed tomography; surface-based: photogrammetry).
374 All materials were treated as isotropic and homogenous. To avoid artificially high stress and
375 strain peaks on the articular and dentary, constraints were not directly applied to the joint
376 region. Instead, an additional component with the same material properties was created to

377 articulate with the joint surface. The morphology of these linking components was based on
378 the cranial articulating joint morphology. The linking components were constrained (15
379 nodes on each side) from translation in x-, y-, and z-direction. To simulate biting at different
380 analogous positions, additional constraints (one node each, in x-, and y- direction, z-direction
381 unrestrained to allow penetration of tooth into prey) were applied to the canine and the
382 posteriormost tooth, each for a unilateral and a bilateral scenario. Muscle forces were
383 assigned according to the calculations taken from the three-dimensional reconstructions
384 (supplementary table S2). As for the MDA, a second set of simulations was performed with
385 all models scaled to the same surface area and muscle forces scaled proportionally to analyse
386 the models at the same relative size³⁴. The models were subsequently imported into Abaqus
387 6.10 (Simulia) for analysis and post-processing. Biomechanical performance of the FE
388 models was assessed via contour plot outputs. In addition, reaction forces (= bite forces) at
389 the bite points and average stress, strain and displacement values per element were obtained
390 from the models.

391 For the simulation of different muscle activation patterns, load forces for the
392 temporalis, the masseter and the pterygoideus groups were varied: each muscle group was set
393 up to successively produce 0, 25, 50, 75 and 100% of the maximum force and all possible
394 permutations were simulated (resulting in $5^3 = 125$ possible combinations, for the five
395 different states and three muscle groups). To automate this process, an R script was used to
396 modify the FEA input files accordingly³⁷. All other settings were kept constant as outlined
397 above and analysed using Abaqus. To compare performances, bite force values and average
398 joint stresses (von Mises, tensile, compressive) were obtained from Abaqus. Average joint
399 stresses were calculated from 30 nodes selected in a grid pattern on the surface of the jaw
400 joint to obtain a maximum spread and analogous point across all taxa. Results of the different

401 muscle activation simulations were plotted in a three-dimensional coordinate system using
402 the freely-available visualisation package Blender (www.blender.org) (Figs. S7-S12).

403 Additional FEA simulations were performed for all taxa scaled to different, discrete
404 mandible lengths: 5, 10, 20, 40, 80, 160 and 320mm. Mandible lengths were chosen to
405 represent the range of sizes observed across the cynodont-mammaliaform transition. Load
406 forces were scaled for each size stage following the $\frac{3}{4}$ power law for each taxon.

407

408 29. Lautenschlager, S. Reconstructing the past: methods and techniques for the digital
409 restoration of fossils. *Royal Soc. Open Sci.* **3**, 160342 (2016).

410 30. Lautenschlager, S. Cranial myology and bite force performance of *Erlikosaurus andrewsi*:
411 A novel approach for digital muscle reconstructions. *J. Anat.* **222**, 260-272 (2013).

412 31. Lautenschlager, S. Estimating cranial musculoskeletal constraints in theropod dinosaurs.
413 *Royal Soc. Open Sci.* **2**, 150495 (2015).

414 32. Thomason, J. J. Cranial strength in relation to estimated biting forces in some mammals.
415 *Canad. J. Zool.* **69**, 2326–2333 (1991).

416 33. Ashman, R. B. & Rho, J. Y. Elastic modulus of trabecular bone material. *J. Biomech.* **21**,
417 177-181 (1988).

418 34. Curtis, N. *et al.* Predicting muscle activation patterns from motion and anatomy:
419 modelling the skull of *Sphenodon* (Diapsida: Rhynchocephalia). *J. Royal Soc. Interface* **7**,
420 153-160 (2010).

421 35. Dumont, E. R., Grosse, I. R., Slater, G. J. Requirements for comparing the performance of
422 finite element models of biological structures. *Journal of Theoretical Biology* **256**, 96-103
423 (2009).

424 36. Bright, J. A. The importance of craniofacial sutures in biomechanical finite element
425 models of the domestic pig. *PLOS one* **7**, e31769 (2012).

426 37. R Core Team (2017). R: A language and environment for statistical computing. R
427 Foundation for Statistical Computing, Vienna, Austria. UR<https://www.R-project.org/>
428